Online ISSN: 2981-0396 Print ISSN: 2981-0388

International Journal of Iron & Steel Society of Iran

Journal Homepage: https://journal.issiran.com/

Research Article

Enhancing Mechanical Performance in GMAW-based WAAM with Fe-rich CuAlNi Electrode Refinement

S. Farzad-Rik *[1], M. Mahmoodi [2], H. Tagimalek [3], M. R. Maraki [4]

[1,2,3] *Faculty of Mechanical Engineering, Semnan University, Semnan, Iran*
[4] *Department of Materials and Metallurgy Engineering, Birjand University of Technology, Birjand, Iran*

ARTICLE INFO

Keywords:

Wire Arc Additive Manufacturing, Gas Metal Arc Welding, Combination Electrodes, Optimization, Taguchi.

Article history:

Received 04 January 2024
Received in revised form 05 Juan 2024
Accepted 06 August 2024

ABSTRACT

Gas metal arc welding (GMAW) based wire-arc additive manufacturing (WAAM) is a promising manufacturing method widely used in various industries. In this study, for the first time, a new type of combined electrode wire with multi-element composition has been designed and developed for arc additive manufacturing of a composite alloy Fe rich-Al-Cu-Ni alloy. GMAW-based WAAM technique technology composed of 4 filaments and 4 elements has the advantages of high deposition efficiency, self-rotation of welding arc, and energy-saving capability. Thin composite alloy walls were fabricated under pure CO_2 gas using GMAW-based WAAM technique technology. To investigate the effect of the parameters introduced by the gas metal arc welding process based on wire arc additive manufacturing, the produced components of the sample layer by layer with different parameters after production are characterized by scanning electron microscope morphologies, X-ray diffraction Microstructural observations of the developed combined electrode reveal (i) BCC and FCC phases, (ii) Good bonding between layers and (iii) defect-free microstructure. Therefore, an experimental design using the Taguchi method was used to determine the parameters affecting the studied properties, including yield strength (YS) and elongation (E). The developed combined electrode alloy exhibits high compression strength (~294 GPa) coupled with high elongation (~0.22%) values (possess both strength and ductility). It has been identified that by varying the heat input via torch travel speed, the microstructure and mechanical properties of the combined electrode can be controlled. Therefore, optimizing GMAW process parameters to produce effective products is of great importance. The experimental results show that voltage and wire speed are the dominant variables that affect the values of YS and E at the test surface. In addition, the contribution of each factor to YS and E was determined. Which can be effectively Corrected with this method.

1. Introduction

Traditionally, an alloy is mainly composed of one dominant element and one or two additional elements and the performance of this alloy are improved by adding other elements in minor amounts. Widespread utilization of additive manufacturing (AM) technologies in high-performance applications require advanced alloys that combine versatile manufacture-ability with excellent mechanical properties [1, 2]. In additive manufacturing (AM), the ability to make items in a straightforward manner by placing materials in one layer on top of another is becoming increasingly popular. In contrast to customary cycles, AM innovation saves approximately half of its creation costs [3, 4]. Therefore, it is considered a savvy, suitable, creative, and solid assembly innovation. The

*Corresponding author
Email: salar.farzad@semnan.ac.ir
Address: Faculty of Mechanical Engineering, Semnan University, Semnan, Iran
1. M. S., 2. Assistant Professor, 3. Ph.D., 4. M. S.

DOI: http://10.22034/IJISSI.2024.2019560.1277
Published by ISSI (Iron & Steel Society of Iran)

most significant advantage of AM is that it can reduce material waste and production time [5]. In recent years, advances in AM technology have enabled the direct production of finished products. Owing to its many benefits, its use is increasing in many fields, including the automotive, aerospace, and electronics industries [6, 7]. AM can be grouped into three categories. direct energy deposition (DED), sheet coating, and powder bed incorporation. Wire arc additive manufacturing (WAAM), which uses wire as an energy source, is a direct energy deposition cycle used in AM innovation [8, 9]. WAAM can be obtained from various additional power sources, such as plasma arc welding, gas tungsten arc welding, and gas metal arc welding (GMAW). GMAW-based WAAM technology is used for achieving high deposition rates, favorable mechanical properties, and low equipment costs without the need for conventional GMAW processes [10]. Among the techniques available for AM, WAAM offers additional advantages. A low initial cost makes it ideal for large-scale production. WAAM is a practical innovation because it allows easy access to components such as wire feeders and soldering irons [11]. Unlike metal powders, the metal wires required for WAAM are readily available and easy to handle. High deposition rates of approximately 8 kg/h were achieved using the GMAW-based WAAM process. High metal deposition limits the surface quality and dimensional accuracy; however, high-volume parts can produce warping and deformation because of the fast deposition rate, high temperature, and excessive energy input. These challenges are often related to additive manufacturing processes. Orbital planning should be studied to obtain favorable process parameters, such as welding speed, wire feed rate, and arc voltage [12].

Zhong et al. [13] examined metal 3D printing and eliminated wire-based arc technology. Their detailed research showed that GMAW-based WAAM is simple and easy to implement because it uses a continuous coil with iron. Other techniques such as plasma arc welding and tungsten inert gas welding require an external wire feeder to obtain the filler metal. Shost et al. [14] conducted a comparative study on the WAAM process. They concluded that the correct selection of design variables and parameter optimization of the WAAM process minimized the residual stress and strain. Tabernero et al. [15] compared performance measurements of different AM-based methods. They showed that their GMAW-based WAAM technology is widely applied to low-cost, large-scale parts production. Many materials can be used to manufacture parts, such as titanium alloys, low-alloy steel, brass, nickel alloys, and aluminum. WAAM consists of three main requirements: movement and arcing systems, wire feeders, and substrates for precision [16, 17]. Bushachi et al. [18] developed a process roadmap for integration into a method, used for defense platforms used by scientists in argon scavengers, stationary gas delivery systems, and heat treatment systems for research. To overcome the problem of shaking, scientists have tried to synchronize the modules so that they can precisely control the components and dimensions of the device. In addition, design guidelines and evaluation methods have been presented to determine the fabrication and manufacturing aspects of structural airship parts [19]. The desired result was obtained using a thicker substrate plate via double-sided WAAM deposition. The corners should be rounded to reduce the visible pressure on the corners and ensure smooth installation. Even after such practice, it was later realized that the WAAM technique was insufficient for complex 3D networks. Similarly, Yuan et al. [20] investigated a method focused on positional beading, a multidimensional drawing and deposition process optimization strategy, and applications in architecture. To obtain the correct path geometry and welding parameters, a parabolic model was developed, which is helpful in determining that the wire speed and value are lower at lower powers and travel speeds. This leads to improved quality and productivity. Therefore, selecting the process parameters with their required levels is necessary to deposit multiple layers in WAAM. Efforts have been made to optimize these process parameters for different steel grades [21, 22]. Vora et al. [23] utilized the WAAM technique based on GMAW to manufacture a multi-facet structure using metal wire on 2.25 Cr-1.0 Mo steel. An advancement method was used to produce appropriate parametric settings of the WAAM variables to develop a slender multi-facet design, and the results showed that the multi-facet design, with a similar dot statement for every bed, was acquired through the enhancement. Kohler et al. [24] consistently analyzed stacked aluminum wires using WAAM and noted changes in bead geometry and design exhibited by interlayer temperature. With increasing wire feed and welding speeds, the layer height decreased and the wall width increased. In addition, there is a high temperature between the sides and the size and height of the aluminum walls.

The studied materials showed that the combination of electrode anomalies and excellent mechanical properties requires fine processing control. It is essential to optimize the WAAM configuration parameters of the yield strength (YS) and elongation (E) using a hybrid electrode droplet. Therefore, the gaps in the above studies were filled by analyzing the combination of electrode structures obtained with the optimized parameterization. In this study, GMAW-based WAAM was used to fabricate and characterize the mechanical properties of a composite electrode structure with Fe-rich CuAlNi wires. In the present study, the best variables of its GMAW-based WAAM process were used to fabricate the composite electrode structures in the present study, the best variables of its GMAW-based WAAM process were used to fabricate the composite electrode structures. The current study focuses on the structural stability and mechanical properties of Fe-rich CuAlNi. This work focuses on the

microstructure, tensile testing, XRD analysis, and scanning electron microscopy (SEM) analysis of Fe-rich CuAlNi. These results are essential for future research and industrial applications. The authors believe that the present study can address industrial problems related to the design and analysis of mechanical properties.

2. Materials and Experimental Method

The configuration of the WAAM framework utilized in this research is displayed in (Fig. 1a.) The WAAM device consists of a GMAW device with a wired device. Iron, copper, nickel, and aluminum combination electrode welding (CEW) with diameters of 0.8, 0.7, 0.3, and 0.1 mm were used in this study (as shown in Fig.1b). The base metal electrode is iron alloy to create the welding arc and copper alloy to stabilize the arc during welding and nickel and aluminum alloys with different diameters are integrated during welding. All examples were made on an St37 steel base plate with dimensions 100×100×10 mm^3 assigned as the substrate material. The chemical composition of the materials and the mechanical properties of the combined electrodes are shown in Tables 1 and 2. In this study, nine experiments of WAAM welding were conducted. Uncontrolled consumable electrodes on the workpiece can result in off-center welds and faulty weld spot connections. The machine is used to move in the X, Y, and Z axis and automate the GMAW process. Due to the use of GMAW welding, the feeding wire electrode is consumable in the form of welding electrode material with a diameter of 1.9 mm. Carbon dioxide (CO_2) is used as a shielding gas.

Table 1. Chemical compound of four consumable wires.

Element	Fe	Cu	Ni	Al	Zn	Mg	Mn	Si	Zr
Iron	Bal	--	--	--	--	--	1.4	0.8	--
Copper	--	Bal	--	--	0.10	0.01	0.40	0.10	0.08
Nickel	--	--	Bal	--	0.25	4.30	0.50	0.40	0.10
Aluminum	--	--	--	Bal	2.4	0.01	3.7	0.04	0.19

Table 2. Mechanical properties of four consumable wires.

Mechanic Properties	Fe	Cu	Ni	Al
Yield strength (N/mm^2)	550	550	>500	125
Elongation (%)	>23	35	>35	17
Tensile strength (N/mm^2)	<420	390-500	>300	275

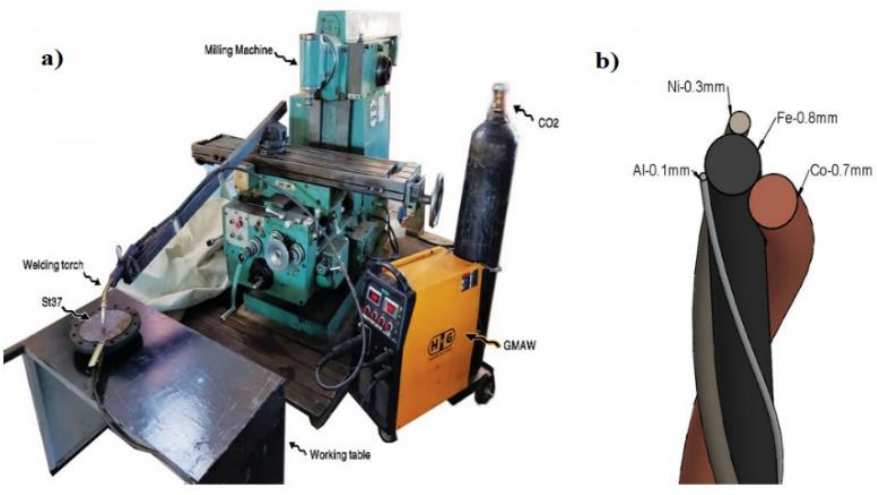

Fig. 1. a) GMAW-based system WAAM device b) 3D model of CEW.

The samples were sanded using 60 to 2500 grit sandpaper and then polished with 0.05 micron alumina powder along with washing liquid on a clean felt and edged for 15 seconds. All samples were sandblasted to remove surface contamination. In this research, input parameters, including welding speed (cm/min), voltage (V), and wire speed (cm/min), were selected as input parameters. Minitab software was used to model and optimize using Taguchi. Standard tensile testing was performed to evaluate the mechanical properties of the optimized parts. For this test, samples were prepared according to ASTM-E8. Their particular shapes and sizes are shown in Fig. 2.

Design of Experiments (DOE) using Taguchi's method is a powerful technique that can determine the optimal combination of factors and parameters from limited data. Using this technique, the measure of the S/N ratio calculation for each process parameter level depends on the property. For quality in S/N analysis, the analysis of variance (ANOVA) technique was performed to check if the process factor was statistically significant. As there are three levels to this experience, L9 orthogonal array, shown in Table 4. was chosen, effectively reducing the total number of samples required to 9.

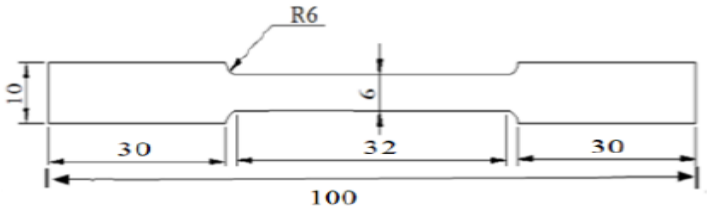

Fig. 2. Standard tensile testing ASTM-E8.

Table 3. Study parameters and their levels.

Levels	Code	parameters		
		Speed welding (mm/min)	Voltage (V)	Wire speed (cm/min)
Low	-1	44	24	5
Medium	0	62	27	6
High	+1	86	32	7

Table 4. Experimental results of Taguchi experimental tests.

Ex	Input parameters			Code		
	Speed welding (mm/min)	Voltage (V)	Wire speed (cm/min)	Speed welding (mm/min)	Voltage (V)	Wire speed (cm/min)
1	44	24	5	-1	-1	-1
2	44	27	6	-1	0	0
3	44	32	7	-1	+1	+1
4	62	24	6	0	-1	0
5	62	27	7	0	0	+1
6	62	32	5	0	+1	-1
7	86	24	7	+1	-1	+1
8	86	27	5	+1	0	-1
9	86	32	6	+1	+1	0

The phase structure of the developed composite electrode was analyzed using X-ray diffraction (XRD) (X' Pert-MPD PRO-PW3040/60 Philips). XRD control, with Cu-Kα radiation, voltage of ~32 kV, and range of 40 ° to 95 ° in 0.02 ° increments, was used. Before examining the microstructure, the samples were sanded continuously with #60 and #2500 sandpaper and cleaned. The element composition and morphology of the grown composite electrodes were investigated using a scanning electron microscope (SEM) (Philips XI30).

3. Results and discussions

3.1. Taguchi analysis

In this research, statistical analysis was performed using Mini-tab 19. Signal-to-noise (S/N) is considered to be placed in a graphical format to understand the result of the input constraints [20]. In this research, the bigger-better relationship was used. The reason for this was to maximize the output effects of mechanical properties. Eq. (1) shows the bigger-is-better relationship.

$$-10 \times \mathrm{Log10}\left(\mathrm{Sum}\frac{\left(\frac{1}{Y^2}\right)}{n}\right) \qquad \text{Eq. (1)}$$

Fig. 3. and Table 5. shows that the YS decreases linearly as the welding speed decreases and then increases sharply. The YS is seen to improve with voltage, whereas the does not vary significantly. The YS expands around a straightforward design as the wire speed increases and diminishes just at the subsequent wire speed. Fig. 3b. shows that the elongation decreases linearly as the welding speed, voltage, and wire speed increase and then again increases sharply.

Table 5. Response obtained from the examination of mechanical properties.

Ex	Responses	
	Yield strength (MPa)	Elongation (%)
1	213.426	0.25
2	285.387	0.156
3	244.309	0.232
4	205.301	0.104
5	234.431	0.19
6	254.474	0.18
7	294.206	0.22
8	225.226	0.124
9	293.327	0.296

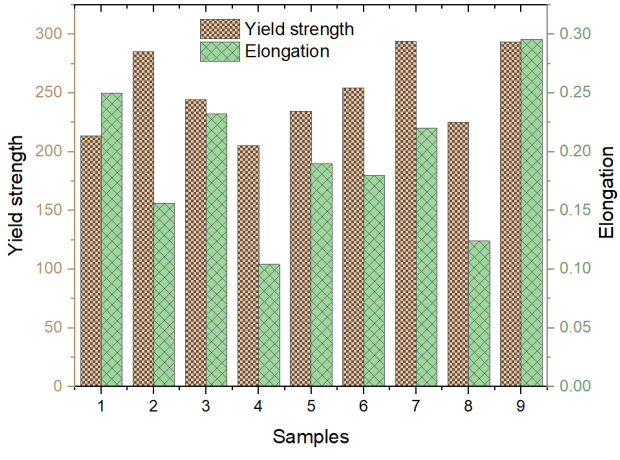

Fig. 3. Stress-strain diagram resulting from tensile test of welded samples.

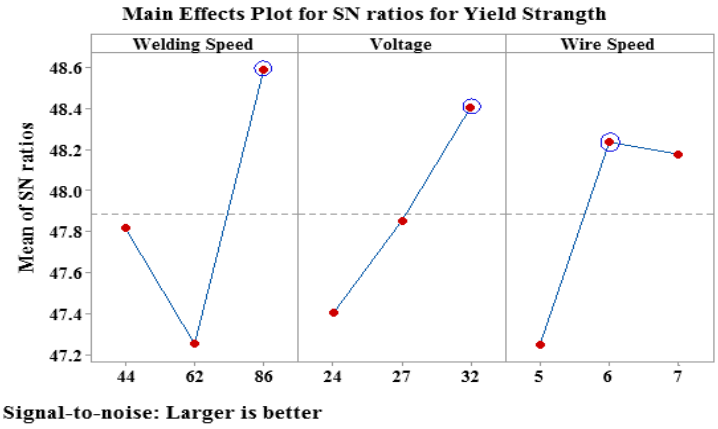

a)

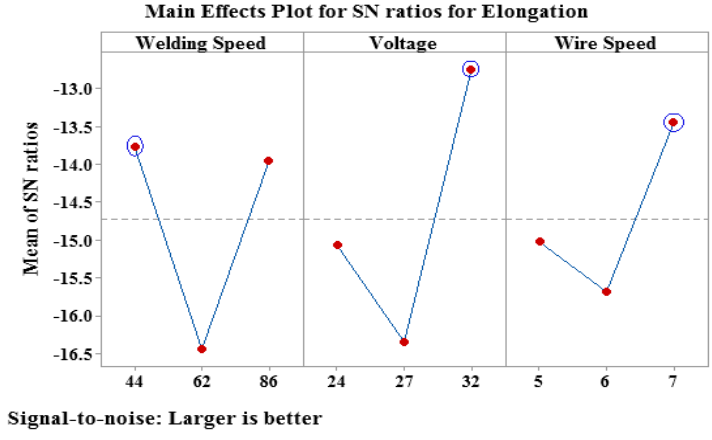

b)

Fig. 4. Plots of the main S/N ratio effects of a) yield strength and b) elongation .

ANOVA identifies the effective process input parameters that affect their characteristics. ANOVA results for changes in yield strength and elongation are shown in Table 6. respectively. In this research, it very well may be seen that on account of yield strength and elongation, wire speed and voltage and welding speed mainly played a role in the P-value smaller than 0.05%. According to the validation test of the optimization, the optimization has a level of reliability response. ANOVA results for the mechanical properties model are R^2 = 0.85, R^2 (adj) = 0.76, and R^2 (predict) = 0.47, respectively. The desirability model is equal to 0.854.

Table 5. shows that welding speed and voltage and wire speed play an essential role in achieving yield strength and elongation changes. Therefore, it clearly shows that wire speed, voltage, and welding speed have the most significant, contribution in achieving maximum yield strength and elongation changes, respectively. Regression conditions were created to lie between the design factors of the GMAW-based WAAM and the welding speed levels and voltage and wire speed responses from the Taguchi technology technique.

Regression of Yield strength = 250.0 - 2.3 Welding Speed_44 - 18.6 Welding Speed_62 + 20.9 Welding Speed _86 - 12.4 Voltage_24 - 1.7 Voltage_27 + 14.0 Voltage_32 - 19.0 Wire Speed_5 + 11.3 Wire Speed_6 + 7.6 Wire Speed_7

Regression of Elongation = 0.1933 - 0.0167 Welding Speed_44 - 0.0367 Welding Speed_62 + 0.0200 Welding Speed _86 - 0.0033 Voltage_24 - 0.0387 Voltage_27 + 0.0420 Voltage_32 - 0.0087 Wire Speed_5 + 0.0113 Wire Speed_6 + 0.02 Wire Speed_7

Fig. 5. shows the interaction effects on welding speed, voltage, and wire speed. The interactions mean of mechanical properties i.e., YS and E, in Fig. 4. shows that the three primary parameters in the DoE are chosen correctly and they affect each other a lot. The results shown in each parameter are as follows: welding speed and voltage have an extreme point, but the opposite has been done in the wire speed. By increasing wire speed, the welding speed of the sample increases significantly and the voltage of the pieces decreases

significantly. The wire speed is the effective parameter on the YS and E of the pieces, and the S/N ratio increases with the increment of the wire speed. The justification for this can be expressed that by lessening the wire speed, porosity is created inside the pieces. For this reason, the YS and E for models with increased wire speed are higher than for models with decreased wire speed. According to the results presented in Table 6. the parameter that had the most negligible impact on YS and E.

Table 6. ANOVA analysis for yield strength and elongation changes.

Welding Source	DF	Adj SS	Adj MS	F-value	P-value	Remarks
Regression	3	9555668913	3185222971	9.76	0.016	significant
Speed welding	1	624064605	624064605	1.91	0.225	
Voltage	1	5380665097	5380665097	16.48	0.010	
Wire speed	1	3550939210	3550939210	10.88	0.022	
Error	5	1632018060	326403612			
Total	8	11187686972				
R-Sq(adj)= 76.66%		R-Sq=85.41%	R-Sq (pred)= 47.78			

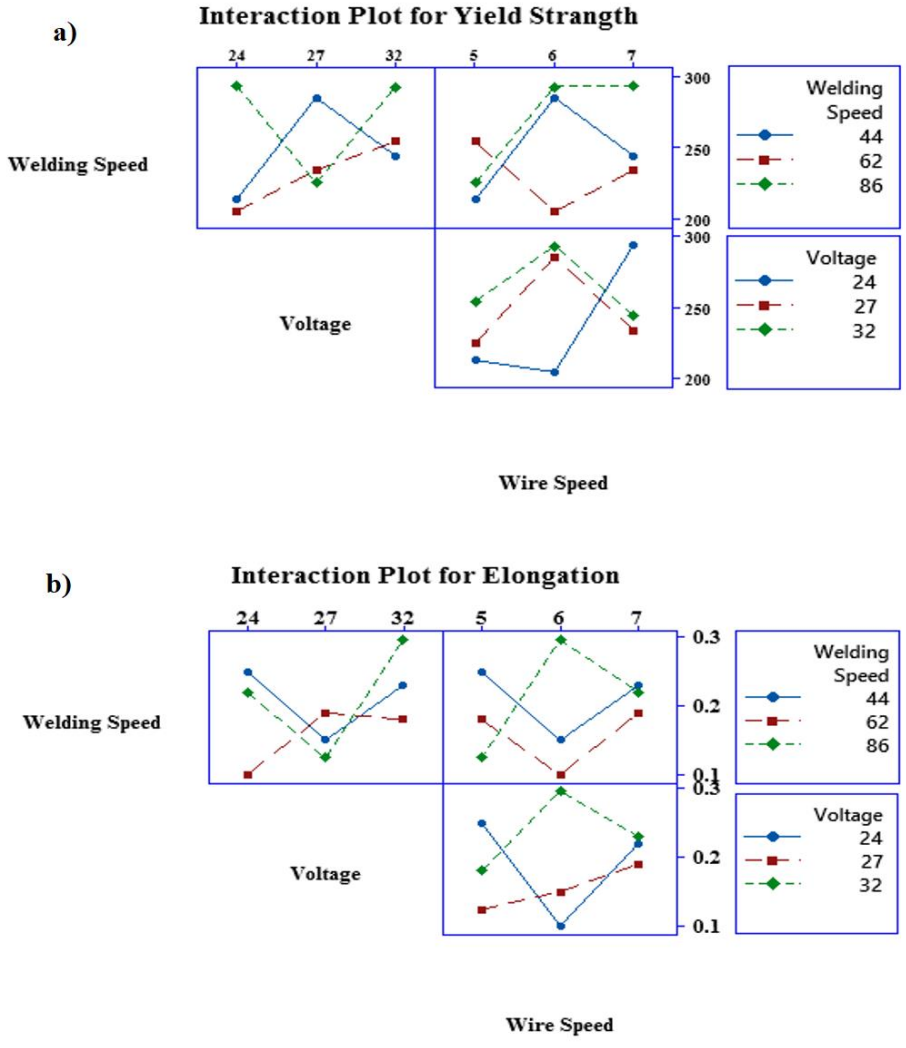

Fig. 5. Interactions of the effect of parameters on; a) yield strength and b) elongation.

Surface plots are an assessment that can be made of the influence of effective process parameters on output parameters, and three-dimensional response level diagrams have been used. In the graphs, two parameters are changed, and the other parameter is kept constant. Three-dimensional surfaces for welding speed, wire speed, and voltage are shown in Figs. 6 and 7.

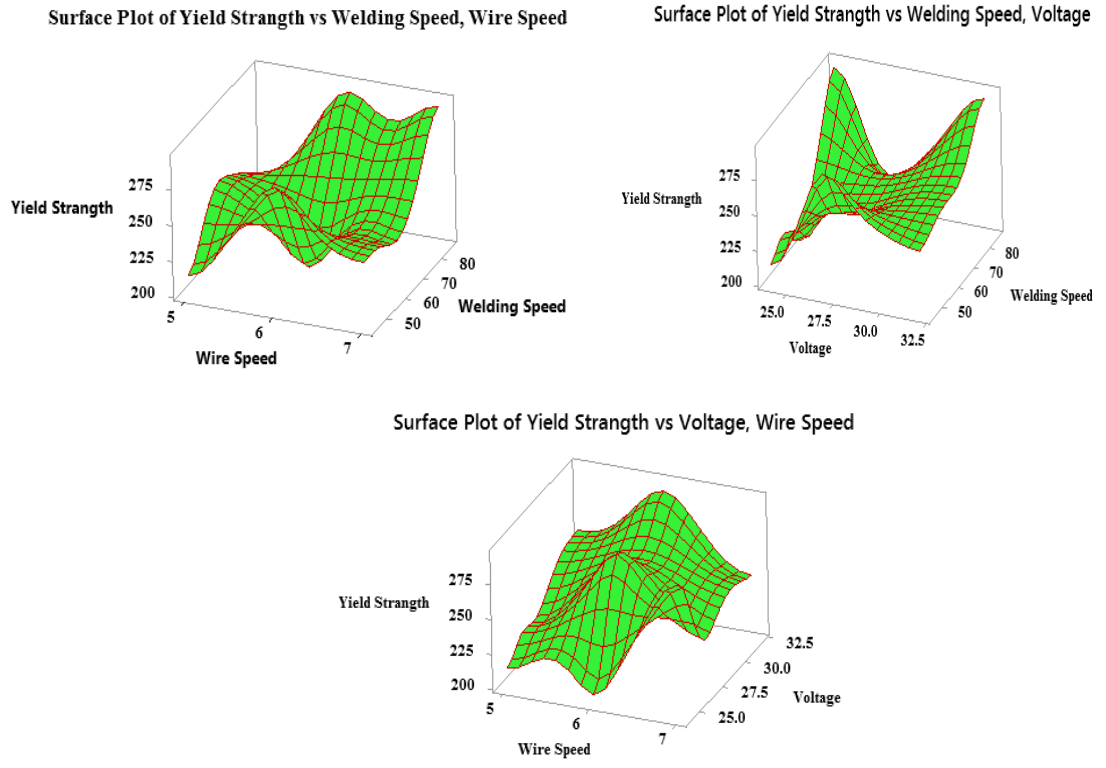

Fig. 6. 3D diagram of parameters affecting yield strength response.

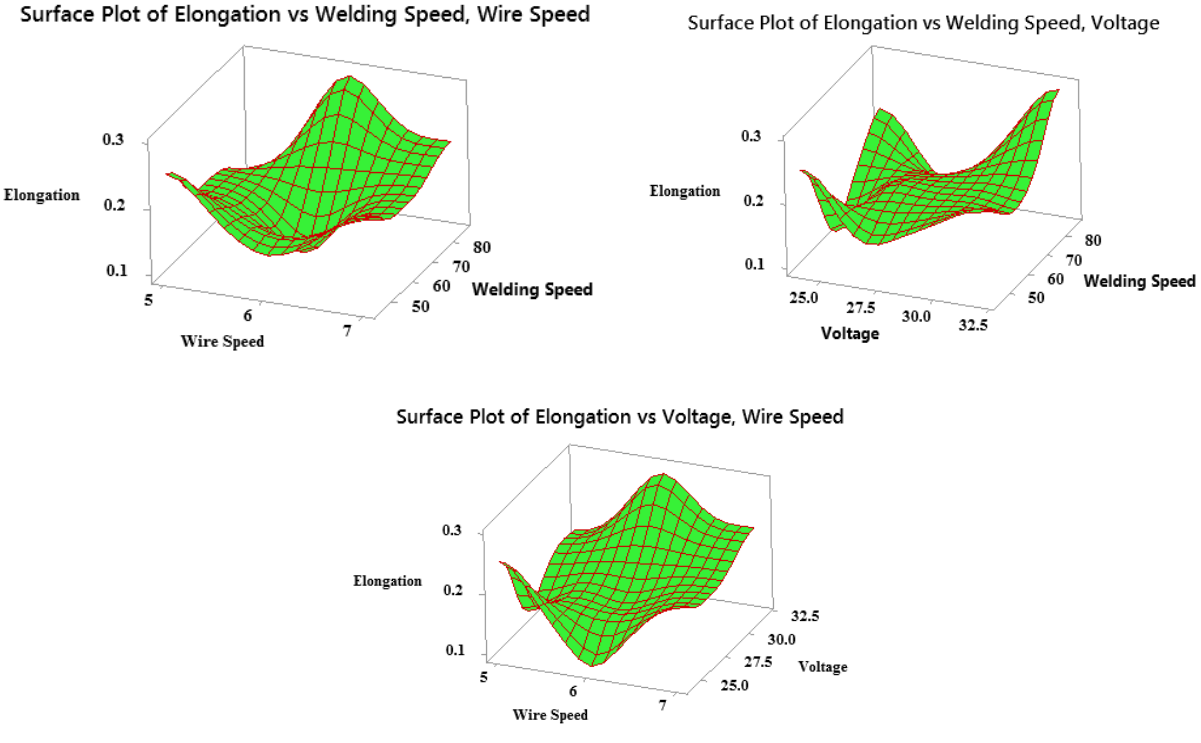

Fig. 7. 3D diagram of parameters affecting Elongation response.

3.2. X-Ray Diffraction Results

Fig. 8. shows the X-Ray Diffraction pattern of the Fe-rich CuAlNi sample prepared by the GMAW-based WAAM method. In the combination of electrodes fabricated by this method, the BCC phase and the FCC phase can be distinguished. An integrated electrode prevents the formation of intermetallic results in single BCC and FCC phases. GMAW-based WAAM models have higher BCC (110) and FCC (200) vulnerabilities. As the welding speed increases, the BCC peak at (110) gradually increases and the BCC peak at (200) decreases. It is clear that the faster the cooling rate, the better the growth of the BCC (110) oriented particles and the more inhibited the development of the BCC (200) oriented particles. The BCC phase is tripped at (100) and (211) and the FCC phase is tripped at (111). From Fig. 8. it can be seen that BCC is the primary phase, and the other phases are the FCC phase in the integrated electrode model.

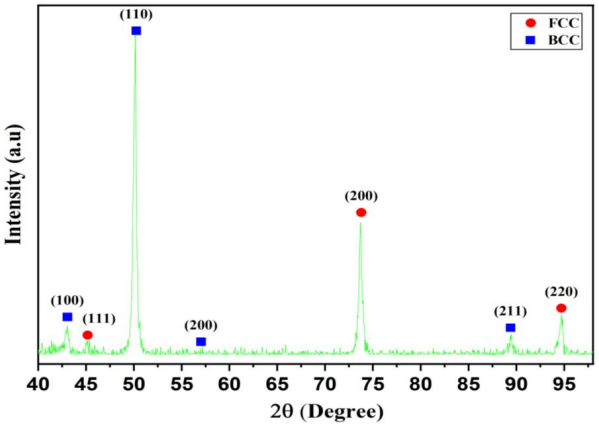

Fig. 8. XRD patterns of the Fe-rich CuAlNi sample produced by the GMAW-based WAAM process.

3.3. SEM Results

SEM images are shown in Fig. 8. The white particles of the second phase are likely disseminated along the grain boundary or dispersed in the grain. The second phase particle is enriched with the light white of aluminum and iron phase and is bordered with dark white color. With more enriched aluminum and iron content but less nickel and copper, the content of second-phase particles with the bright white color of grain boundary phase gradually increases, one of the essential factors of welding energy that can cause possible reactions between alloys. In addition, the melting during welding also causes cavities and porosity of different sizes. By increasing the welding speed, the void has become smaller, and the size of the grain boundaries has increased. By welding speed up, the shaped molten pool has increased, which reduces the cooling rate. This factor increases the grain boundaries and makes the structure coarser. By decreasing the welding voltage, the amount of heat produced in the welding area is reduced, and this factor increases the cooling rate and reduces the grains size created. (The increase in the warmth created with the welding speed has an inverse relationship and a direct relationship with the voltage of the welding wire). The lower the welding voltage, the lower the arc length. the amount of penetration, and the stability of the welding arc fluctuates as the heat increases and the formation of cavities and porosity in the area of the welding grain boundaries increases. The phases are mainly distributed along the grain boundaries in a pure form in the Al-Ni matrix. By increasing the iron content and decreasing the copper content, Al-Ni phases are produced and dispersed as points on the cross-sectional surface of the grain boundaries or inside the grains. From other SEM observations, it was found that the dendritic areas are entirely smooth, and no significant features are observed in them. The analysis showed that the level of alloy elements in the dendritic and inter-dendritic regions differs in all three alloys. The story of Al-Ni-Cu in the dendritic areas was relatively lower, while the inter-dendritic areas of the alloy appeared rich in iron. However, the number of deposits was relatively small, and no significant difference was seen in the distribution of Fe deposits from the surface to the core of the sample. SEM observations also showed that the Fe-rich deposits have circular or oval morphology. The Fe-Al-Ni-Cu alloy image by SEM shows that the Fe-Al-Ni-Cu alloy has a relatively uniform grain size distribution. On other hand, black needle-shaped areas in these images indicate porosity, and white areas indicate alloy matrix. It was found that the porosity distribution was uniform for most of the samples. But as the percentage of enriched iron increases, the porosity decreases. With increasing welding speed, the grains become more significant, and the needle ferrite and Widmanstätten ferrite decrease. Austenite is essentially needle-shaped with different morphologies. When the needles thin and elongate, they are called Widmanstätten Austenite (WA). When more unusual and more common, it is called isotropic austenite (AA). Intra-grain austenite (IA) is also observed, which characterizes the structure of the welded part, the ratio of which varies according to the maximum temperature achieved and the cooling rate. A decrease in particle size is observed due to low temperature. Therefore, the cell granule morphology is clearly observed in the austenitic surrounding the ferrite grains. This morphology is preferred because austenitic is harder than ferrite and prevents any cracks in the ferritic region from spreading to other grains. This is because the melting temperature in the solder is higher and the cooling rate is faster. This structural change is characteristic of the fusion welding process. By increasing the heat input, the particle size is reduced. There is no dividing line between the molten region and the

molten metal. By increasing the welding speed, it can be said that the welding input heat is reduced and the solder puddle is more minor, causing cooling expansion due to the temperature difference. These agents make the structure more minor and increase the grain boundaries, improving its mechanical properties.

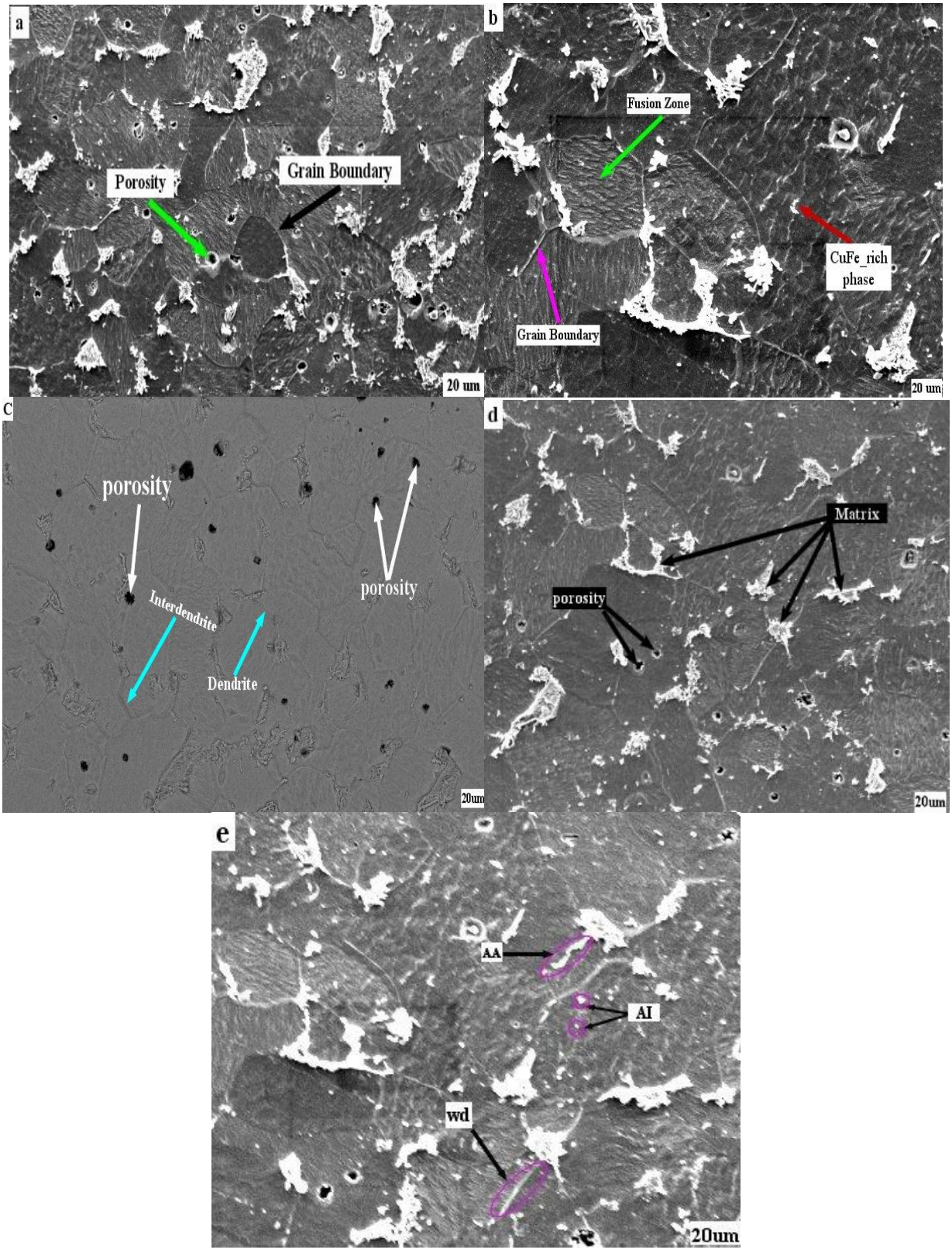

Fig. 9. SEM images of Fe-rich CuAlNi sample produced by the GMAW-based WAAM process.

4. Conclusions

An investigation was conducted to optimize welding parameters for the GMAW-based WAAM process on Fe-rich CuAlNi. The three parameters wire speed, welding speed, and voltage affect the yield strength and elongation. A summary of the results:

- According to the S/N ratio, the best compound to maximize performance, YS, and E in any Fe-rich CuAlNi sample is from the voltage and welding speed.
- To improve the GMAW-based WAAM parameters, the Taguchi method provides an efficient experimental design.
- The optimal process parameters were YS, welding speed of 86 mm/min, voltage of 32 V, and wire speed of 6 cm/min.
- ANOVA was used for statistical analysis. For the welding voltage and wire speed, the regression model is important as the interaction term, while the regression model term has a significant influence on the welding voltage response. The normal probability plot provided a good statistical analysis for ANOVA and better future results than those of the proposed model.
- The optimal process parameters are E, welding speed of 44 mm/min, voltage of 32 V, and wire speed of 7 cm/min.
- By increasing the welding speed, the particles become finer, and the Widmanstätten ferrite content decreases.
- The higher the welding voltage, the greater the length and penetration of the arc, and the stability of the arc fluctuates as heat increases. Therefore, the amount of weld spatter and voiding in the weld area increased.

Author Contributions

Farzad-Rik and Tagimalek planned the scheme, initiated the project and suggested the experiments; Farzad-Rik and Mahmoodi conducted the experiments and analyzed the empirical results; Mahmoodi and Maraki developed the mathematical modeling and examined the theory validation. The manuscript was written through the contribution of all authors. All authors discussed the results, reviewed and approved the final version of the manuscript.

Acknowledgments

The authors are very much thankful to the unknown reviewers for their valuable and constructive suggestions which improved the readability of the paper.

Conflict of Interest

The authors declared no potential conflicts of interest with respect to the research, authorship and publication of this article.

Funding

The authors received no financial support for the research, authorship and publication of this article.

References

[1] Olakanmi E.O, Cochrane R.F, Dalgarno K.W, A review on selective laser sintering/melting (SLS/SLM) of aluminium alloy powders: Processing, microstructure, and properties, Progress in materials science.2015; 74: 401-477.

[2] DebRoy T, Wei H.L, Zuback J.S, Mukherjee T, Elmer J.W, Milewski J.O, Beese A.M,Wilson-Heid A, De A, Zhang W, Additive manufacturing of metallic components–process, structure and properties, Progress in Materials Science. 2018; 92: 112-224.

[3] Rosli N.A, Alkahari M.R, bin Abdollah M.F, Maidin S, Ramli F.R, Herawan S.G, Review on effect of heat input for wire arc additive manufacturing process, Journal of Materials Research and Technology. 2021; 11: 2127-2145.

[4] Korkmaz M.E, Waqar S, Garcia-Collado A, Gupta M.K, Krolczyk G.M, A technical overview of metallic parts in hybrid additive manufacturing industry, Journal of Materials Research and Technology.2022; 18: 384-395.

[5] Senthil T, Babu S.R, Puviyarasan M, Dhinakaran V, Mechanical and microstructural characterization of functionally graded Inconel 825-SS316L fabricated using wire arc additive manufacturing, Journal of Materials Research and Technology. 2021; 15: 661-669.

[6] Chaudhary B, Jain N.K, Murugesan J, Patel V, exploring temperature-controlled friction stir powder additive manufacturing process for multi-layer deposition of aluminum alloys, Journal of Materials Research and Technology. 2022; 20: 260-268.

[7] Nguyen H.D, Pramanik A, Basak A, Dong Y, Prakash C, Debnath S, Shankar S, Jawahir I.S, Dixit S, Buddhi D, A critical review on additive manufacturing of Ti-6Al-4V alloy: microstructure and mechanical properties, Journal of Materials Research and Technology. 2022; 18: 4641-4661.

[8] Hu Z, Qin X, Li Y, Yuan J, Wu Q, Multi-bead overlapping model with varying cross-section profile for robotic GMAW based additive manufacturing, Journal of Intelligent Manufacturing. 2020; 31: 1133-1147.

[9] Shen B, Lu J, Wang Y, Chen D, Han J, Zhang Y, Zhao Z, Multimodal-based weld reinforcement monitoring system for wire arc additive manufacturing, Journal of Materials Research and Technology.2022; 20: 561-571.

[10] Dinovitzer M, Chen X, Laliberte J, Huang X, Frei H, Effect of wire and arc additive manufacturing (WAAM)

process parameters on bead geometry and microstructure, Additive Manufacturing.2019; 26: 138-146.
[11] Aldalur E, Suárez A, Veiga F, Thermal expansion behaviour of Invar 36 alloy parts fabricated by wire-arc additive manufacturing, Journal of Materials Research and Technology.2022; 19: 3634-3645.
[12] Henckell P, Gierth M, Ali Y, Reimann J, Bergmann J.P, Reduction of energy input in wire arc additive manufacturing (WAAM) with gas metal arc welding (GMAW), Materials. 2020; 13: 2491.
[13] Antonysamy A, Microstructure, texture and mechanical property evolution during additive manufacturing of Ti6Al4V alloy for aerospace applications, The University of Manchester, United Kingdom. 2012.
[14] Stavinoha J.N, Investigation of plasma arc welding as a method for the additive manufacturing of Ti-6Al-4V alloy components, Montana Tech of the University of Montana. 2012.
[15] Ermakova A, Mehmanparast A, Ganguly S, A review of present status and challenges of using additive manufacturing technology for offshore wind applications, Procedia Structural Integrity. 2019; 17: 29-36.
[16] Dongqing Y, He C, Zhang G, forming characteristics of thin-wall steel parts by double electrode GMAW based additive manufacturing, Journal of Materials Processing Technology. 2016; 227: 153-160.
[17] Azadi Moghaddam M, Golmezergi R, Kolahan F, Multi-variable measurements and optimization of GMAW parameters for API-X42 steel alloy using a hybrid BPNN–PSO approach, Measurement. 2016; 92: 279-287.
[18] Yang L, Keng H, Brian B, Donald G, Francisco M, Mamballykalathil M, Soeren W, Additive manufacturing of metals: the technology, materials, design and production, Springer. 2017.
[19] Zhang Z, Chengshuai S, Xinkun X, Liming Liu, Surface quality and forming characteristics of thin-wall aluminium alloy parts manufactured by laser assisted MIG arc additive manufacturing, International Journal of Lightweight Materials and Manufacture. 2018; 1: 89-95.
[20] Zengxi P, Donghong D, Bintao W, Dominic C, Huijun L, John N, Arc welding processes for additive manufacturing: a review, Transactions on intelligent welding manufacturing, Springer .2018: 3-24.
[21] Panchagnula J.S, Suryakumar S, Manufacture of complex thin-walled metallic objects using weld-deposition based additive manufacturing, Robotics and Computer-Integrated Manufacturing. 2018; 49: 194-203.
[22] Park J.H, Kim S.H, Moon H.S, Kim M.H, Influence of Gravity on Molten Pool Behavior and Analysis of Microstructure on Various Welding Positions in Pulsed Gas Metal Arc Welding, Applied Sciences. 2019; 9: 4626.
[23] Vora J, Parikh N, Chaudhari R, Patel V.K, Paramar H, Pimenov D.Y, Giasin K, Optimization of bead morphology for GMAW-based Wire-arc additive manufacturing of 2.25Cr-1.0 Mo steel using metal-cored wires, Applied Sciences. 2022; 12: 5060.
[24] Köhler M, Jonas H, Klaus D, Effects of thermal cycling on wire and arc additive manufacturing of Al-5356 components, Metals. 2020; 10: 952.